LAWRENCE
LIVERMORE
NATIONAL
LABORATORY

UCRL-JRNL-212272

The Study of Optically Induced Effects due to Bending and Twisting using Vector Finite Element Method

Jennifer Dacles-Mariani, Garry Rodrigue

May 13, 2005

Computational Methods in Applied Mechanics and Engineering

The Study of Optically Induced Effects due to Bending and Twisting using Vector Finite Element Method

Jennifer Dacles-Mariani and Garry Rodrigue
Department of Applied Science
University of California Davis, California 95616

Abstract

We study the effects of macroscopic bends and twists in an optical waveguide and how they influence the transmission capabilities of a waveguide. These mechanical stresses and strains distort the optical indicatrix of the medium producing optical anistropy. The spatially varying refractive indices are incorporated into the full-wave Maxwell's equations. The governing equations are discretized using a vector finite element method cast in a high-order finite element approximation. This approach allows us to study the complexities of the mechanical deformation within a framework of a high-order formulation which can in turn, reduce the computational requirement without degrading its performance. The optical activities generated, total energy produced and power loss due to the mechanical stresses and strains are reported and discussed.

Index Terms

Variable refractive index, bending and torsion, Maxwell's equations, optical fiber,vector finite element.

I. Introduction

The vector finite element method is one of the more popular numerical methods to date because of its ability to discretely represent complex geometries and complex materials while maintaining component continuity of the discrete fields. In recent papers Reiben et al. [1], a high-order finite element approximation of the Maxwell's equations has been reported and used to model optical fiber propagation. A high-order discretization can reduce the mesh size, CPU time requirement and memory usage for a given problem without sacrificing its accuracy. In the field of electromagnetics, optical fibers and transmission lines are subject to structural stresses and strain which can degrade their performance. Generating the computational mesh for these deformed structures accurately is one of the challenges encountered in numerically simulating complex geometries. This is where the vector finite element method is highly useful.

Mechanical strain in the form of bending and/or twisting of optical fibers are routinely encountered during normal operation that these effects are actively studied to date. These macroscopic effects can attenuate the transmitted or propagated electromagnetic fields and can result in power loss. Currently, the studies done in this field are mostly theoretical and combined analytical/numerical. It would be interesting to include these mechanical strains in the analysis of an optical pulse propagating inside an optical fiber using the full-wave Maxwell's equations.

This is the subject of our study; to analyze the effect of bending and/or twisting of an optical fiber complete with its core and cladding. Specifically, we would like to isolate the stress-optical effects present under these circumstances, report the optical activities we see and discuss what happens to the power inside the core. We start by modifying an existing full-wave Maxwell's equations code [1], to include the spatially varying refractive indices due to bending and/or twisting. The full-wave Maxwell's equations code contains the high-order finite element approximation and high-order energy conserving time integration method that allows us to reduce the total number of mesh points without sacrificing accuracy and still remain conservative. This code has been successfully applied to other electromagnetics studies. Two relevant studies, one on optical anisotropy induced by torsion and bending [2], the other on bending losses [3], gave guidelines on how the optical indicatrix is distorted due to the mechanical strains. We adopt their findings and include the spatially varying refractive indices in our code.

Next, we study the different optical fiber configurations starting from a straight optical fiber and progressing to different bending angles.

This work was performed under the auspices of the U.S. Department of Energy by the University of California, Lawrence Livermore National Laboratory under contract No. W-7405-Eng-48,and under the U.S. AFOSR Contract No. F49620-01-0327.

University of California, Davis and Institute for Scientific Computing Research, Lawrence Livermore National Laboratory, daclesmariani1@llnl.gov,ghrodrigue@ucdavis.edu

Corresponding author: Tel.(925)422-4032,Fax(925)422-7819

In another computation set-up, we introduce a varying range of uniformly applied twist angle on the fiber. Finally, we generate a twisted and bent fiber and propagate an optical pulse inside it.

We use a Gaussian approximation of the fundamental mode as the input optical pulse that is launched in one end of the fiber. We then allow this pulse to propagate for a short period of time and investigate the optical activities introduced by bending and/or twisting.

II. High-Order Vector Finite Element Formulation of Coupled First-order Maxwell's Equations

Electromagnetic fields are fully characterized by the electric field intensity, $\mathbf{E}$, and the magnetic flux density, $\mathbf{B}$. These fields are generated by sources and are supported in a given medium. Maxwell's equations fully describe their spatial and temporal relationships between these fields, their sources and the medium.

In this section, an overview of the high-order finite element formulation is presented. Details of the formulation and general application can be found in Ref. [4].

The coupled first-order Maxwell's equation is given by:

$$\epsilon \frac{\partial \mathbf{E}}{\partial t} = \nabla \times (\mu^{-1}\mathbf{B}) - \sigma \mathbf{E} - \mathbf{J}(t) \tag{1}$$

$$\frac{\partial \mathbf{B}}{\partial t} = -\nabla \times \mathbf{E} - \sigma^{\star}(\mu^{-1}\mathbf{B}) \tag{2}$$

here $\mathbf{J}$ is the current density vector; σ and $\sigma^{\star}$ are the electric and magnetic conductivity respectively. The fictitious magnetic conductivity is introduced to facilitate the application of the Perfectly Matched Layer condition. In addition, ϵ and μ are the permittivity or dielectric tensor and the inverse magnetic permeability tensor, respectively. Typically, these parameters are scalar and they represent simple materials that are linear, istoropic and homogeneous. But in some cases the value of this parameter is more complicated where they can be tensor functions as in a non-linear medium. This is what happpens when we consider the effects of the mechanical stresses and strains during the bending and twisting processes, where we allow the value of ϵ to be independent of time but dependent in space.

A Galerkin finite element procedure with 1-form ($Curl$ - conforming) vector basis functions to discretely represent the electric field intensity is adopted. The magnetic flux density is represented using a 2-form (or Div - conforming) vector basis function.

The high-order and energy conserving time-integration of Eqns. (1) and (2) are given by a generalized symplectic update, [1] as

$$M_{\epsilon}\frac{\partial e}{\partial t} = K^{T} M_{\mu} b - M_{\sigma} e - M_{\epsilon} j \tag{3}$$

$$\frac{\partial b}{\partial t} = -Ke - M_{\sigma}^{\star} \tag{4}$$

where e and b represent the discrete differential 1-form and 2-form electric and magnetic fields respectively. The rectangular matrix representing the discrete curl operator is K, and j is the discrete 2-form time dependent current source. M_{*} are symmetric positive definite (SPD) mass matrices computed using the appropriate basis functions and material property functions. Finally, the instantaneous electromagnetic energy is the numerical version of the total energy given by

$$\tilde{\mathcal{E}} = e_{T} M_{\epsilon} e + b^{T} M_{\mu} b \tag{5}$$

In this study, a third-order polynomial basis function is used. By doing so, we were able to reduce the PML region to a single layer by defining appropriate cubic tensor functions of space, and then "projecting" these functions over the single element PML layer. We also adopted the use of symplectic integrators for the ordinary differential equations which resulted in more accurate time averaged energy conservation. The method has also been proven to reduce the effect of numerical dispersion.

III. Elasto-optic effects

Now that we have the discrete equation framework, the next step is to include the elasto-optic effects. Elasto-optic effects are the changes in the refractive index of an optical fiber in response to a mechanical stress. When an optical fiber or transmission line is subjected to a mechanical stress or strain such as bending, torsion or both, the medium becomes anisotropic such that the optical behavior along the fiber axis differs from that along the perpendicular axis. This difference can be seen as the amount of distortion in the optical indicatrix due to any external field. The optical indicatrix is an important means of visually looking at how the refractive index varies with direction in a given medium or substance. For isotropic materials, the indicatrix is a sphere and the refractive index is the same in all direction.

Let $\nu = \epsilon^{-1}$ be the impermeability tensor. That is,

$$\sum_k \eta_{ik}\epsilon_{kj} = \delta_{ij} \tag{6}$$

The optical indicatrix is defined as the "surface"

$$\sum_{ij} \eta_{ij}x_i x_j = 1 \tag{7}$$

The amout of distortion in the indicatrix due to any external field or change of material is rather small, and the distorted indicatrix is still an ellipsoid. The distortion manifest themselves as a change in the lengths of the major and minor axes as well as a rotation of the axes. If we let

$$\sum_{ij} \tilde{\eta}_{ij}x_i x_j = 1 \tag{8}$$

be the new ellipsoid, then the difference satisfies

$$\sum_{ij} \Delta_{ij}x_i x_j = 0. \tag{9}$$

Since

$$\Delta(\sum_k \eta_{ik}\epsilon_{kj}) - \sum_k \eta_{ik}\epsilon_{kj} = \sum_k (\eta_{ik} + \Delta\eta_{ik})(\epsilon_{kj} + \Delta\epsilon_{kj}) - \sum_k \eta_{ik}\epsilon_{kj} = \sum_k \Delta\eta_{ik}\epsilon_{kj} + \sum_k \eta_{ik}\Delta\epsilon_{kj} = 0 \tag{10}$$

Hence,

$$\Delta\epsilon_{kl} = -\sum_i \Delta\eta_{ik} \sum_k \epsilon_{kj} \tag{11}$$

Thus, once the changes $\Delta\eta_{ij}$ are known, the changes $\Delta\epsilon_{ij}$ can be computed. The changes of the coefficients in the optical indicatrix under the action applied stress is given by

$$\begin{bmatrix} \Delta\eta_{11} \\ \Delta\eta_{22} \\ \Delta\eta_{33} \\ \Delta\eta_{23} \\ \Delta\eta_{31} \\ \Delta\eta_{12} \end{bmatrix} = \begin{bmatrix} p_{11} & p_{12} & p_{13} & p_{14} & p_{15} & p_{16} \\ p_{11} & p_{12} & p_{13} & p_{14} & p_{15} & p_{16} \\ p_{11} & p_{12} & p_{13} & p_{14} & p_{15} & p_{16} \\ p_{11} & p_{12} & p_{13} & p_{14} & p_{15} & p_{16} \\ p_{11} & p_{12} & p_{13} & p_{14} & p_{15} & p_{16} \\ p_{11} & p_{12} & p_{13} & p_{14} & p_{15} & p_{16} \end{bmatrix} \begin{bmatrix} S_{11} \\ S_{22} \\ S_{33} \\ S_{23} \\ S_{31} \\ S_{12} \end{bmatrix} \tag{12}$$

In the case of linear strains

$$S_{ij} = \frac{1}{2}(\frac{\partial u_i}{\partial x_j} + \frac{\partial u_j}{\partial x_i}) \tag{13}$$

where $u = [u_1\ u_2\ u_3]^t$ is the displacement vector.
In the case of silica

$$\begin{bmatrix} p_{11} & p_{12} & p_{13} & p_{14} & p_{15} & p_{16} \\ p_{21} & p_{22} & p_{23} & p_{24} & p_{25} & p_{26} \\ p_{31} & p_{32} & p_{33} & p_{34} & p_{35} & p_{36} \\ p_{41} & p_{42} & p_{43} & p_{44} & p_{45} & p_{46} \\ p_{51} & p_{52} & p_{53} & p_{54} & p_{55} & p_{56} \\ p_{61} & p_{62} & p_{63} & p_{64} & p_{65} & p_{66} \end{bmatrix} = \begin{bmatrix} p_{11} & p_{12} & p_{12} & 0 & 0 & 0 \\ p_{12} & p_{11} & p_{12} & 0 & 0 & 0 \\ p_{12} & p_{12} & p_{11} & 0 & 0 & 0 \\ 0 & 0 & 0 & (p_{11} - p_{14})/2 & 0 & 0 \\ 0 & 0 & 0 & 0 & (p_{11}p_{12})/2 & 0 \\ 0 & 0 & 0 & 0 & 0 & (p_{11} - p_{12})/2 \end{bmatrix} \tag{14}$$

where $p_{11} = 0.121, p_{12} = 0.270$.

IV. Twisting Effects

When a fiber is twisted, it produces two effects, birefringence rotation and mechanical torsion [5], [6]. It causes a rotation τz of the cross-sectional plane z, where τ is the twist angle in radians. We consider the simple problem of the torsion of a straight fiber optic of circular cross section. Under the torque, the fiber twists. Let the cross section at $z = 0$ be fixed and α be the rotation of a section at $z = 1$ relative to that at $z = 0$. The displacement of a particle located at (x, y, z) is, in polar coordinates,

$$u_r = 0,\ \ u_\theta = \alpha z r,\ \ u_z = 0 \tag{15}$$

or, in Cartesian coordinates

$$u_x = -\alpha z y,\ \ u_y = \alpha z x,\ \ u_z = 0 \tag{16}$$

The linear strain components are:

$$S_{12} = 0 \;\; S_{13} = -12\alpha y \;\; S_{23} = 12\alpha x \tag{17}$$

Then,

$$\begin{bmatrix} \Delta\eta_{11} \\ \Delta\eta_{22} \\ \Delta\eta_{33} \\ \Delta\eta_{23} \\ \Delta\eta_{31} \\ \Delta\eta_{12} \end{bmatrix} = \begin{bmatrix} 0 \\ 0 \\ 0 \\ 1/2(p_{11}-p_{12})\alpha x \\ -1/2(p_{11}-p_{12})\alpha y \\ 0 \end{bmatrix} \tag{18}$$

Moreover,

$$\Delta\epsilon = -\epsilon(\Delta\eta)\epsilon = -\epsilon^2 \begin{bmatrix} 0 & 0 & -\frac{1}{2}(p_{11}-p_{12})\alpha y \\ 0 & 0 & \frac{1}{2}(p_{11}-p_{12})\alpha x \\ -\frac{1}{2}(p_{11}-p_{12})\alpha y & \frac{1}{2}(p_{11}-p_{12})\alpha x & 0 \end{bmatrix} \tag{19}$$

The refractive indices are given by

$$n_1 = n_{co} \tag{20}$$

where n_{co} = refractive index of the core.

$$n_2 = n_{co}\left\{1 + \frac{n_{co}^2}{4}(p_{11}-p_{12})\sqrt{\frac{\tau^2 r^2}{4}}\right\} \tag{21}$$

$$n_3 = n_{co}\left\{1 - \frac{n_{co}^2}{4}(p_{11}-p_{12})\sqrt{\frac{\tau^2 r^2}{4}}\right\} \tag{22}$$

Notice that the spatial variation in the core refractive index is due only to radial variations.

V. Bending effects

In case of the a tensile stress applied parallel to the fiber axis, i.e., fiber bending, the optical fiber is compressed on the inner part of the fiber and stretched on the outer part. The bend is characterized by a bending radius R which is defined as $R = Total\ length/(Bend\ angle)$ With the bending stress, only $S_{33} \neq 0$. Then,

$$\begin{bmatrix} \Delta\eta_{11} \\ \Delta\eta_{22} \\ \Delta\eta_{33} \\ \Delta\eta_{23} \\ \Delta\eta_{31} \\ \Delta\eta_{12} \end{bmatrix} = \begin{bmatrix} p_{12}S_{33} \\ p_{12}S_{33} \\ p_{11}S_{33} \\ 0 \\ 0 \\ 0 \end{bmatrix} \tag{23}$$

and

$$\Delta\epsilon = -\epsilon(\Delta\eta)\epsilon \tag{24}$$

$$\Delta\epsilon \;\; = -\epsilon^2 \begin{bmatrix} p_{12}S_{33} & 0 & 0 \\ 0 & p_{12}S_{33} & 0 \\ 0 & 0 & p_{11}S_{33} \end{bmatrix} \tag{25}$$

The corresponding refractive indices are

$$n_1 = n_{co}(1 + \frac{n_{co}^2 p_{12} x}{2R}) \tag{26}$$

$$n_2 = n_{co}\left\{1 + \frac{n_{co}^2(p_{11}+p_{12})x}{4R} + \frac{n_{co}^2}{4}(p_{11}-p_{12})\sqrt{\frac{x^2}{R^2}}\right\} \tag{27}$$

$$n_3 = n_{co}\left\{1 + \frac{n_{co}^2(p_{11}+p_{12})x}{4R} - \frac{n_{co}^2}{4}(p_{11}-p_{12})\sqrt{\frac{x^2}{R^2}}\right\} \tag{28}$$

These refractive indices show variation in the bending direction only (x-direction) and the bending radius R.

VI. Combined bending and torsion effects

The fiber which undergoes bending and twisting will have a combined effect that is linearly superimposed.

$$\Delta\epsilon = -\epsilon(\Delta\eta)\epsilon = -\epsilon^2 \begin{bmatrix} p_{12}S_{33} & 0 & -\frac{1}{2}(p_{11}-p_{12})\alpha y \\ 0 & p_{12}S_{33} & \frac{1}{2}(p_{11}-p_{12})\alpha x \\ -\frac{1}{2}(p_{11}-p_{12})\alpha y & \frac{1}{2}(p_{11}-p_{12})\alpha x & p_{11}S_{33} \end{bmatrix} \tag{29}$$

The resulting refractive index along the three principal axes are:

$$n_1 = n_{co}(1 + \frac{n_{co}^2 p_{12} x}{2R}) \tag{30}$$

$$n_2 = n_{co}\left\{1 + \frac{n_{co}^2(p_{11}+p_{12})x}{4R} + \frac{n_{co}^2}{4}(p_{11}-p_{12})\sqrt{\frac{x^2}{R^2} + \frac{\tau^2 r^2}{4}}\right\} \tag{31}$$

$$n_3 = n_{co}\left\{1 + \frac{n_{co}^2(p_{11}+p_{12})x}{4R} - \frac{n_{co}^2}{4}(p_{11}-p_{12})\sqrt{\frac{x^2}{R^2} + \frac{\tau^2 r^2}{4}}\right\} \tag{32}$$

The combined effect implies a more complicated variation radially, as well as linearly in the x-direction.

VII. Computational Results

In this section, we discuss the details of our computational simulations. First, we modify the existing computer code to include the spatially varying form of the refractive indices. Both the core and the cladding are allowed to have the new modified refractive indices that contains the effects of the mechanical strains. Next, we construct a computational domain consisting of a core with diameter of $10\ microns$, and the cladding with a diameter of $80\ microns$. The core has a refractive index of 1.471 while the cladding has 1.456. The optical fiber has a length of $155\ microns$. The computational domain is decomposed into a computation mesh consisting of hexahedral elements. Since we are using the high-order finite element formulation, the mesh size for these runs are comparatively small but still accurate. We use a mesh size of 151,117 with 147,200 elements. In the formulation of the high-order approximations, a high-order polynomial basis functions of degree $p = 2$ along with a high-order symplectic (energy conserving) integrator of order $k = 3$ is chosen.

To complete the computational set-up, we impose a Perfect Electic Conductor (PEC) conditions on the outer cladding and an absorbing boundary condition at the exit end of the mesh.

At the start of the calculation, we launch a pulsed voltage source on one side of the fiber which is excited both spatially and temporally. The spatial dependence is a Gaussian approximation of the fundamental propagating mode in a circular fiber, [7]. One advantage of using this approximation as opposed to the full modal distribution for a single mode operation in a circular fiber is that it's application is straightforward allowing for a less cumbersome application of the input pulse. The temporal dependence is a pulsed sine wave containing 20 wavelengths.

We evolve the input pulse in time using a leap-frog method which is widely used because it is both conditionally stable and non-dissipative.

In the following table, we list the computational runs we considered. For the bent fiber, we performed four different bending angles ranging from 15^0 to 60^0. The bending radii, R, are also listed. Four different twisting angles are also performed ranging from $\pi\ radians$ to $100\ \pi\ radians$. Finally, a combined 15^0 bend and $20\ \pi/length$ twist is also considered. We found that we don't preserve the uniformity of the mesh if the fiber is bent over 60^0 and if the fiber is twisted over $100\pi\ radians/micron$.

To track the optical activities, we monitor and report the total energy, electromagnetic field and power inside the core.

TABLE I
Computational Experiments

Straight Fiber	–	–	–	–
Bent Fiber	$15^0, (R = 592.05\ microns)$	$30^0, (R = 296.03\ microns)$	$45^0, (R = 197.35\ microns)$	$60^0, (R = 148.01\ microns)$
Twisted Fiber	$\pi\ radians/micron$	$20\pi\ radians/micron$	$60\pi\ radians/micron$	$100\pi\ radians/micron$
Bent and Twisted Fiber	$15^0, (R = 197.35\ microns)$	$20\pi\ radians/micron$	–	–

Figs. 1 and 2 show the computational meshes for a bent and a twisted fiber, respectively which were generated using TrueGrid, [8]. A mesh relaxation scheme was implemented during the generation process in order to ensure that a uniformly varying mesh is produced.

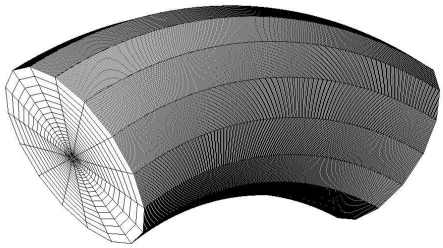

Fig. 1. Computational Mesh for a Bent Fiber.

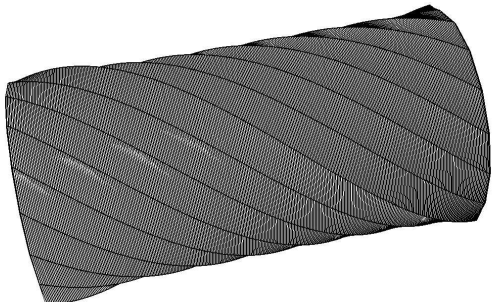

Fig. 2. Computational Mesh for a Twisted Fiber.

In the straight fiber simulation, Fig. 3, we propagate the approximated fundamental mode for up to $1.0\ picoseconds$ and $155\ microns$ and track the power inside the core. Here, we computed the power $\mathbf{P}$ as the magnitude of the Poynting field, $log_{10}\sqrt{\mathbf{P}\cdot\mathbf{P}}$ where $\mathbf{P}=\mathbf{E}\times\mathbf{B}$ at a given time. The weakly guided pulse travels unattenuated for the given length of time and space. The power inside the core increases as it travels in the core and reaches a maximum value of $0.6\ kW/micron^2$. The power level is sustained throughout the rest of the simulation which implies that there is no significant power loss observed for this short propagation period.

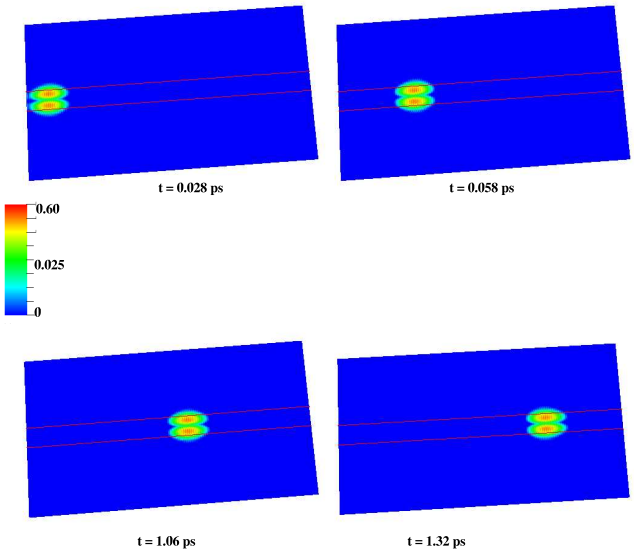

Fig. 3. Power flow in $kW/micron^2$ inside a straight fiber.

Bending of an optical fiber is known to cause attenuation in the signal resulting in power loss. The change in the refractive index of the core implies that along the core-cladding interface, when the core refractive index value becomes lower than the cladding refractive index, the light leaks out which subsequently contributes to the loss of power in the core. To start, the straight fiber mesh is subjected to varying bend angles as mentioned above. In a 15^0 bend (Fig. 4), a plot of the power inside the core shows that as the input pulse evolves in time, the core power begins to leak out into the cladding. In Fig.5, a 60^0 bend shows that the input pulse actually leaves the core into the cladding and gets guided back into the core. However, as the bend angle is progressively increased (Fig.6), as we track the progression of the pulse in time, we see that the cladding guides the pulse back into the core. We notice that a bend in an optical fiber introduces optical activity that is asymmetric and dependent in favor of the bending direction (x-direction).

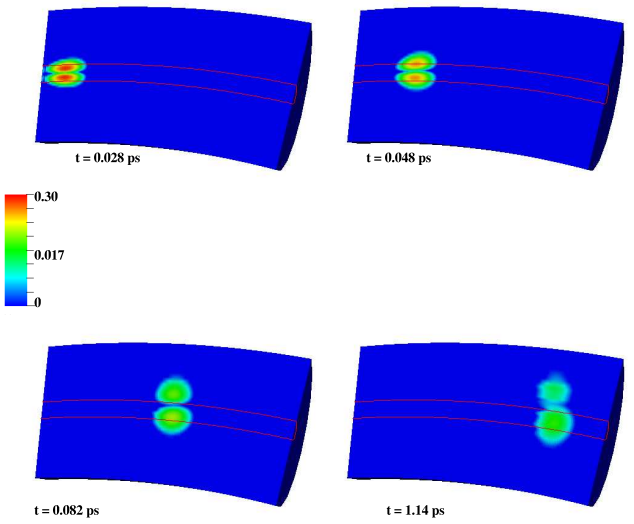

Fig. 4. Power flow in $kW/micron^2$ in a 15-degree bend.

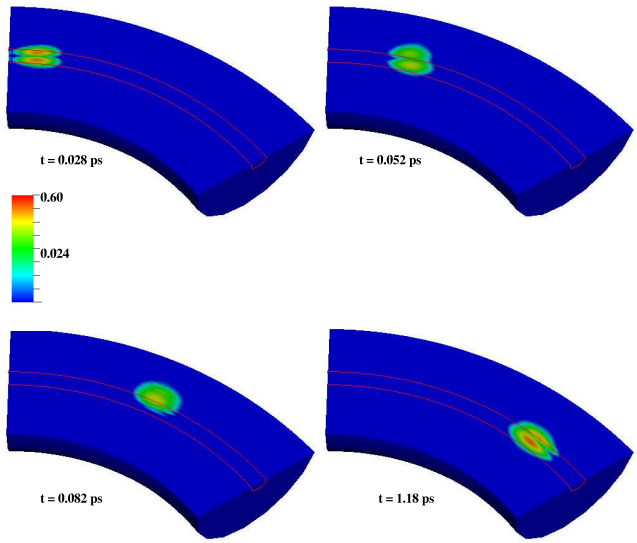

Fig. 5. Power flow in $kW/micron^2$ in a 60-degree bend.

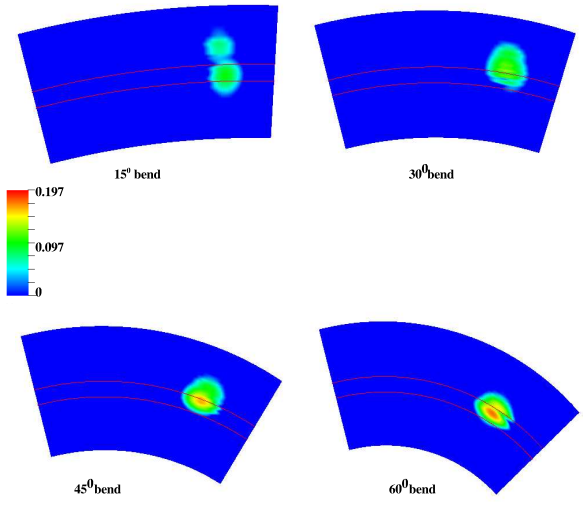

Fig. 6. Power flow in $kW/micron^2$ for 15-degree, 30-degree, 45-degree and 60-degree at t = 0.128 ps.

In another plot, Fig.7, we show the electromagnetic field at increasing time periods and cross-section. Note that the electromagnetic field starts out symmetric and proceeds to distort as it propagate in space and time. The section of the fiber experiencing compression on the left side of the graphics (inner side of optical fiber) and the section experiencing tension is on the right side (outer side of optical fiber).

In Fig. 8, we plot the instantaneous normalized energy which shows that the a maximum value is reached but as the input pulse continues to propagate close to the bend, it suffers the maximum amount of leakage. However, note that some power is gained back as the input pulse moves away from the bend, then starts to get guided back into the core.

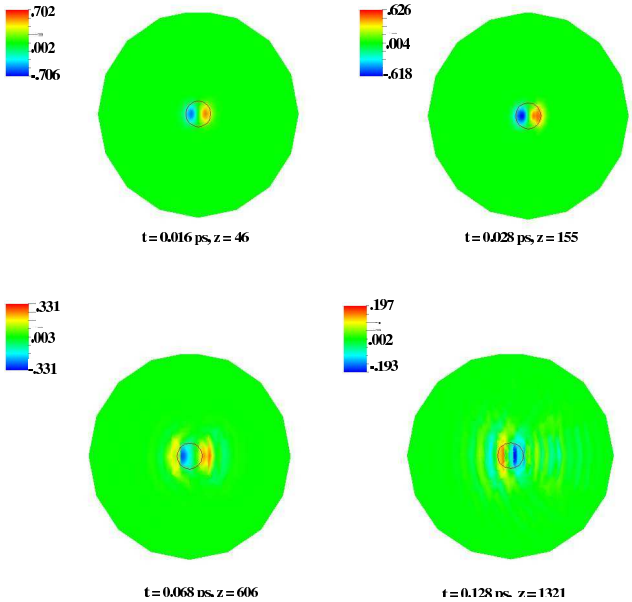

Fig. 7. Electric field propagation in $kV/micron$ for 15-degree bend.

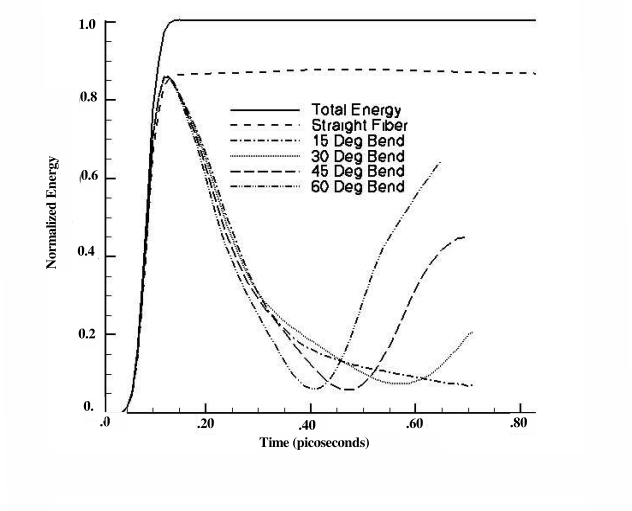

Fig. 8. Comparison of time evolution of total energy for a bent fiber.

When a uniform twist τ is applied to a fiber which is originally straight, it produces a twist induced birefringence [8],

$$[h]\alpha = g\tau \tag{33}$$

where $g = -n_0^2 p_{44}$. Here, $P_{44} = (p_{11} - p_{12})/2 = -.075$, $n_0 \simeq 1.46$ for fused silica, $g \simeq 0.16$ for weakly doped single-mode fiber of arbitrary index profiles. For a different type of fused silica (more doping), then a different value for g will result.

The existence of this optical activity is apparent in the following figures which supports the finding in the paper by Ulrich [4]. Another distinguishing property of twisting the fiber is that the optical property change is only dependent on the radial coordinate. In Fig. 9, we show how the input optical pulse leaks out radially from the core to the cladding in a symmetric fashion. The optical activities are also most noticeable when the electromagnetic field E_y is plotted as a function of time and space. Note that the optical pulse starts out similar to the straight fiber but changes as it propagate in space and evolve in time. In Fig. 10, we see the pulse leaking out of the core in a circular pattern which continues to disperse into the core as the pulse propagates down the fiber.

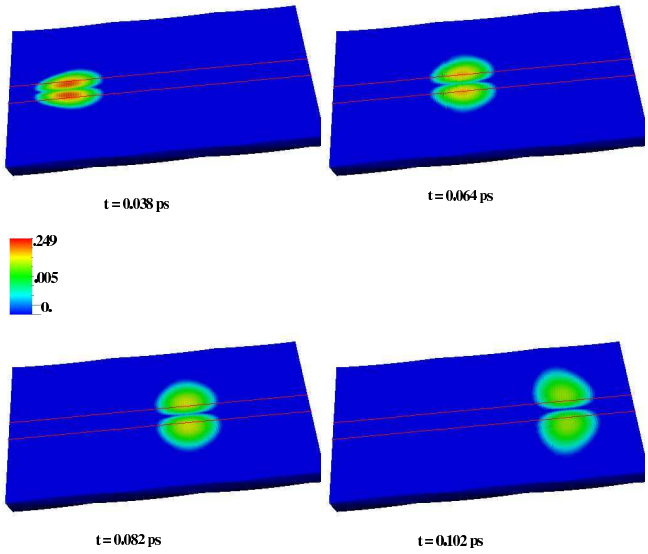

Fig. 9. Power flow in $kW/micron^2$ for a 20pi twist fiber.

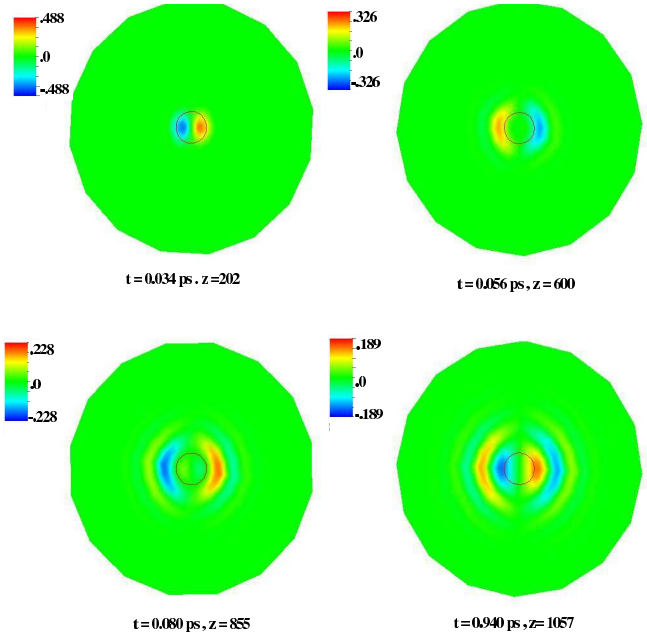

Fig. 10. Electric field propagation in $kV/micron$ for a twisted fiber.

The instantenous normalized energy are given in Figure 11. Note that unlike the bent fiber, the input pulse is not re-guided back into the core.

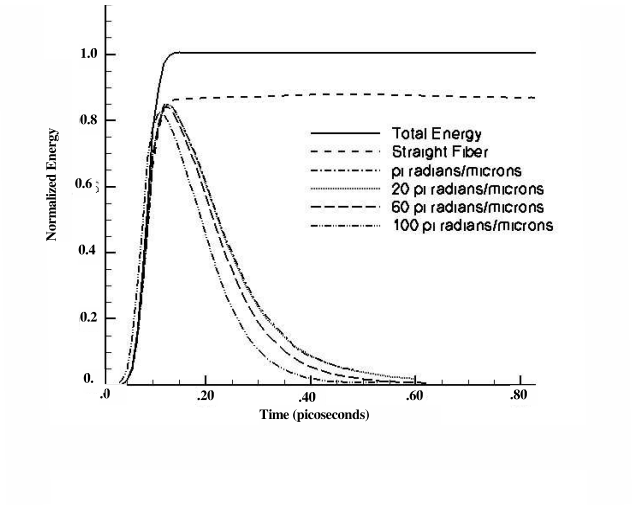

Fig. 11. Comparison of time evolution of total energy for a twisted fiber.

Finally, the combined bending and twisting leads to a more complicated pattern. The optical activity depends both on the radial and on local field points. Fig. 12 shows the electromagnetic field variation, while Fig. 13 illustrates the power comparison between a 15^0 bend, a 20π twist, and the combined effect.

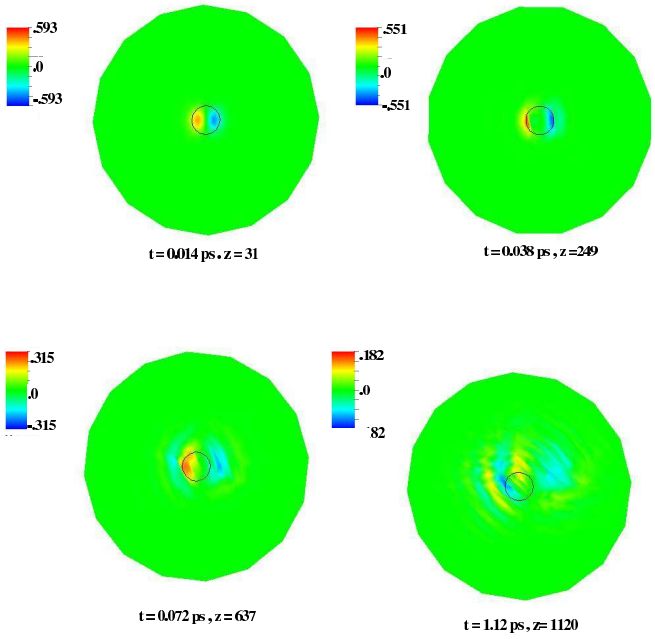

Fig. 12. Electric field propagation in $kV/micron$ for 20pi twist.

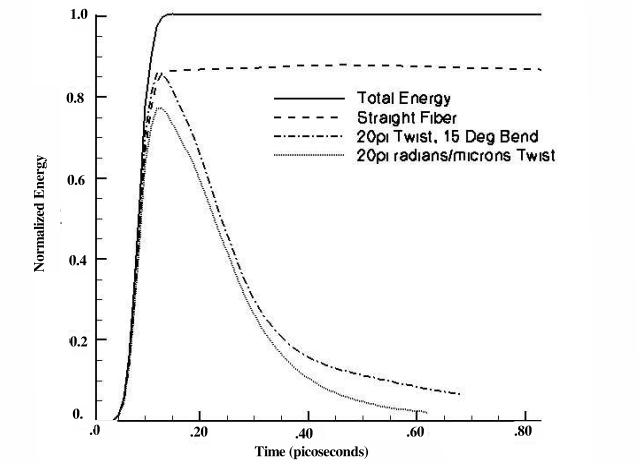

Fig. 13. Comparison of time evolution of total energy in the core between a bent fiber, a twisted fiber and a combined bent and twisted fiber.

VIII. Concluding Remarks

Mechanical strains due to bending and twisting are investigated using the full-wave Maxwell's equations which is modified to include spatially varying refractive indices. The equations are discretized using vector finite element method with high-order finite element approximation. A straight single-mode optical fiber which propagates an approximated fundamental mode is subjected to different bend angles and twist angles. In the bending case, we found that the optical activity starts as a function of the bending direction (x-direction). This finding supports previous work done on this subject. We also found that higher bend angles allow the input pulse to be guided back into the core. Twisting the fiber, on the other had, results in a more symmetric pattern which becomes circular as the pulse travels down the fiber. The twisting effect produces a circular, symmetric dispersion which is dependent on the radial variation. Finally, the combined bending and twisting produces a more complex pattern that includes both the bending direction and radial direction.

References

[1] R. Rieben,D. White, G. Rodrigue*High Order Symplectic Integration Methods for Finite Element Solutions to Time Dependent Maxwell Equations*,
[2] H. Tai, R. Rogowski *Optical anisotropy induced by torsion and bending in an optical fiber*, Optical Fiber Technology 8(2002), 162-169.
[3] G. Durana,J. Zubia, J. Arrue, G. Aldabaldetreku,and J. Mateo *Dependence of bending losses on cladding thickness in plastic optical fibers*, Optical Society of America, 2003.
[4] R. Rieben *A Novel High Order Time Domain Vector Finite Element for the Simulation of Electronic Device*, Ph.D. thesis, University of California, Davis, 2004 UCRL-TH-205466..
IEEEhowto:kopka M. Li, X. Chen *Fiber Spinning for Reducing Polarization Mode Dispersion in Single Mode Fibers: Theory and Applications*, Optical Fiber Technology 8(2002), 162-169.
[5] R. Ulrich, A. Simon *Polarization optics of twisted single-mode fibers*, Optical Fiber Technology 8(2002), 162-169.
[6] G. Agrawal, *"Nonlinear Fiber Optics"*, Third Ed, 2001.
[7] XYZ Scientific Applications Inc, "TrueGrid home page", *http://www.xyz.com*, 2002.